BUTTERWORTH HEINEMANN

Direct numerical simulation of a turbulent flow in a channel having periodic pressure gradient

Yutaka Miyake, Koichi Tsujimoto, and Hideki Beppu
Department of Mechanical Engineering, Osaka University, Osaka, Japan

The intent of this paper is to contribute database information for a flow less complicated than a backward step flow and less simple than a flat channel flow, demonstrating the influence of pressure gradient in an internal flow and serving to stimulate the creation of new improved turbulence models. A direct numerical simulation (DNS) was conducted for a turbulent channel flow having a periodic pressure gradient; i.e., a channel having flat plate walls, a solid one on one side and a porous one on the other side, which allows variable strength injection/suction of fluid. The Reynolds number based on the mean friction velocity on the two walls and the half width of the flow passage is 300. The mean flow field as well as such statistical quantities of turbulence as fluctuation velocities, and Reynolds stresses are presented, with a discussion of the influence of the periodic pressure gradient. The energy budget for the transport equations for the turbulent stresses is also included. The momentum balance is given in sections normal to the mean flow. It is demonstrated that although the thin layer approximation is valid, the pressure gradient effect in this flow is different from that in a boundary-layer flow.

Keywords: channel flow; turbulence; pressure gradient; direct numerical simulation; database; turbulence models

Introduction

Construction of highly reliable turbulence models is an urgent and keen problem for computational fluid dynamics of today. To this point, validation of many kinds of proposed models and their improvement have been conducted mainly using simple canonical flows, such as decaying homogeneous turbulent flow, two-dimensional (2-D) channel flow, etc. Although remarkable progress has been achieved, and many turbulent models are implemented in computational codes used in engineering, further improvement and new models are still needed. Although the work requires testing models in complex flows, overly complex flows such as backward step flow are not necessarily suitable as reference flows, because, for example, a backward step flow includes too many flow elements within a small space. In view of this, we investigate a channel flow having a periodic pressure gradient in this paper.

Flows having a periodic pressure gradient have attracted the attention of various investigators. Many of their studies are concerned with both boundary layers in the flow along an indented wall (Zeman and Jensen 1987; Hunt et al. 1990) and internal flows (Frederick and Hanratty 1988; Patel et al. 1991), but the flow we are concerned with is one along a flat plate of a 2-D channel having a periodic pressure gradient. Some reports of experimental investigations of this flow are available (Sano and Asako 1991; Sano 1992; Miyake and Nakashima 1993), but no numerical simulations have been presented, other than than the previous study by these authors (Kajishima and Miyake 1992).

A series of studies of this type of flow conducted by the present authors includes both experimental (Miyake and Nakashima 1993) and numerical approaches (Kajishima and Miyake 1992). In the present report, a numerical approach involving direct numerical simulation (DNS) of a turbulent flow in a 2-D flat channel with a periodic streamwise pressure variation is presented. The pressure gradient is introduced by assuming injection/suction of fluid from one of the walls, which is assumed to be flat and porous.

Similar large-scale simulation has been conducted by large-eddy simulation (LES) using a grid number of 1.22×10^6, for low Reynolds number slightly higher than the present DNS. The present simulation is intended to reconfirm the findings of the LES in the layer close to the wall in order to establish the influence of a varying pressure gradient on the near-wall turbulence, because in LES, the small-scale structures of turbulence and the dissipation rate are less accurate than required for testing models because of the subgrid scale models. The flow is expected to be capable of incorporating the effects of pressure gradient, upstream memory, different time scale of perturbation, etc., but not in an overly complicated manner.

In a boundary-layer flow, the outer region is not significantly affected by the change of the flow condition on the wall (Nagano et al. 1993). Therefore, it is possible to conduct flow simulation parabolically, from one section to the next, consecutively. Then, a one-dimensional (1-D) calculation is sufficient for the boundary-layer flow, even if it has pressure gradient in the flow direction. However, in this flow, the flow in the core region, which is largely modified by the streamwise pressure gradient (as described in the main body of this text), must be sufficiently

Address reprint requests to Prof. Y. Miyake, Department of Mechanical Engineering, Osaka University, 2-1 Yamada-oka, Suita, Osaka 565, Japan.

Received 18 January 1995; accepted 16 June 1995

Int. J. Heat and Fluid Flow 16: 333–340, 1995

655 Avenue of the Americas, New York, NY 10010

0142-727X/95/$10.00
SSDI 0142-727X(95)00053-S

accurate to obtain the correct wall friction, because the turbulent mixing in the core region controls the wall friction. Thus, for this flow, a good model of the core region and of the near-wall region is needed. Furthermore, for this elliptic-type flow, both the models and the numerical schemes must be valid at every point in the flow field. That is, a small change in the turbulence structure and/or a small error in a limited area can seriously degrade the performance of the turbulence models. Therefore, as a flow for testing turbulence models, this flow presents a more severe challenge than those considered in the past.

Numerical procedure

The governing equation is the set of three-dimensional (3-D) Navier–Stokes equations. The computational code for this work, which is based on a spectral method fundamentally similar to that presented by Kim et al. (1987), was written specifically for this problem. Kim et al. converted the equations of momentum and mass into equations of wall-normal vorticity and wall-normal velocity, which are fourth-order differential equations, and mass conservation. In this paper, instead of the vorticity equation, streamwise and spanwise momentum equations are used. Thus, pressure appears explicitly as an unknown. The coordinate system and the computational domain are shown in Figure 1.

A Cartesian coordinate system is employed, in which x, y, z or $x_i (i = 1, 2, 3)$-axis are the streamwise, normal, and spanwise directions, respectively, and the velocity components in the respective directions are denoted by u, v, w or $u_i (i = 1, 2, 3)$. The computational domain is a rectangular volume with a wall separation $H_y = 2\delta$, a streamwise length $H_x = 4\pi\delta$, and a spanwise width $H_z = \pi\delta$.

As boundary conditions, periodic conditions are applied in the streamwise and spanwise directions. Both top ($y = 2\delta$) and bottom ($y = 0$) walls are flat and are subject to a no-slip condition. The wall is assumed to be porous with injection/suction of varying intensity of fluid in order to generate a periodic pressure gradient. In this simulation, the normal velocity on the porous wall is given by

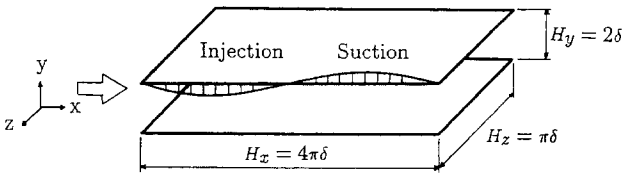

Figure 1 Computational flow field and coordinate system

$$v_0 = -0.5 \sin\left(\frac{2\pi x}{H_x}\right) \tag{1}$$

The spatial discretization is a Fourier series expansion in x and z, and a Chebyshev polynomial expansion in the normal direction. Time advancement is done by a semi-implicit method (Crank–Nicolson scheme for the viscous term and third order Adams–Bashforth scheme for the convective term).

The Reynolds number $\mathrm{Re}_\tau = \bar{u}_\tau \delta/\nu$ is 150 where $\bar{u}_\tau$ is the mean friction velocity of the two walls; i.e., $\bar{u}_\tau = [(\bar{\tau}_u + \bar{\tau}_l)/2\rho]^{1/2}$ where $\bar{\tau}_u$ and $\bar{\tau}_l$ are wall friction stresses on the upper and lower walls, respectively. Because the friction velocity of the solid wall is smaller than that of the porous one, the Reynolds number based on the mean friction velocity ($\hat{u}_\tau$) of the solid (lower) wall is 122.

The grid number is $128 \times 129 \times 64$ in x, y, z, and the resulting grid separations given in Table 1 in which the superscript $^+$ means quantities nondimensionalized by using $\bar{u}_\tau$ and ν, the kinematic viscosity. In addition to the above wall units, other wall units are defined. Those using $\bar{u}_\tau$ and ν are denoted with a superscript $\hat{}$, for example, for the quantity A, by $\hat{A}^+$.

Notation

A	flatness parameter, $1 - 9A_2/8 + 9A_3/8$ $A_2 = b_{ij}b_{ij}$, $A_3 = b_{ij}b_{jk}b_{ki}$
b_{ij}	anisotropic tensor, $\overline{(u_i'u_j')}/k - (2/3)\delta_{ij}$
C_{ij}	convection rate, $-\bar{u}_k\overline{(u_i'u_j')}_{,k}$
C_p	nondimensional pressure coefficient, $(p - p_0)/\rho\hat{u}_\tau^2$
D_{ij}	dissipation rate, $-2\nu\overline{u_{i,k}'u_{j,k}'}$
H_x, H_z	streamwise and spanwise length of computational domain
J_{Pij}	pressure diffusion rate, $-\delta_{ik}\overline{p'u_j'} + \delta_{jk}\overline{p'u_i'})_{,k}$
J_{Tij}	turbulent diffusion rate, $-\overline{(u_i'u_j'u_k')}_{,k}$
J_{Vij}	viscous diffusion rate, $-\nu\overline{u_i'u_j'}_{,kk}$
k	turbulent kinetic energy, $\overline{u_k'v_k'}/2$
P_{ij}	production rate, $-(\overline{u_j'v_k'}\bar{u}_{i,k} + \overline{u_i'v_k'}\bar{u}_{j,k})$
R_t	turbulent Reynolds number, $k^2/\nu\epsilon$
Re_τ	Reynolds number, $\bar{u}_\tau\delta/\nu$
t	time
$\bar{u}_\tau$	mean friction velocity of two walls, $[(\bar{\tau}_u + \bar{\tau}_l)/2\rho]^{1/2}$
$\hat{u}_\tau$	mean friction velocity of lower wall, $[\bar{\tau}_l/\rho]^{1/2}$
u, v, w	velocity components in x, y, and z directions, respectively
$\overline{u_i'u_j'}$	Reynolds stress
x, y, z	streamwise, wall-normal, and spanwise directions, respectively
$\hat{y}^+$	nondimensional distance from wall, $\hat{u}_\tau y/\nu$

Greek

β	nondimensional pressure gradient, $(\nu/\rho\hat{u}_\tau^3)(\partial p/\partial x)$
δ	half width of channel
δ_{ij}	Kronecker delta
ϵ	dissipation rate of turbulent energy
ν	kinematic viscosity
ρ	density
$\bar{\tau}_u$, $\bar{\tau}_l$	wall friction stress on upper and lower wall, respectively
ϕ_{ij}	redistribution rate, $\overline{p'(u_{i,j}' + u_{j,i}')}$

Indices

$(\hat{A})^+$	nondimensionalized quantity $(\bar{A})$ by $\hat{u}_\tau$ and ν
$(\bar{A})$	ensemble average over z-direction and time
$(A)'$	fluctuating component
$(A)_k$	components with respect to turbulent energy transport equation
$(A)_{,t}$	time differentiation
$(A)_{,i}$	spatial differentiation with respect to i-coordinate.

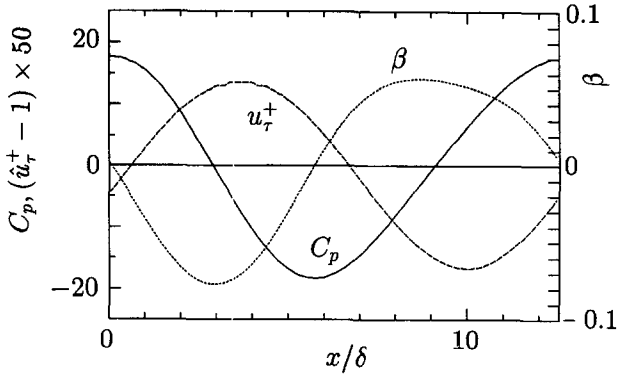

Figure 2 Variation of friction velocity $u_\tau^+ = u_\tau / \hat{u}_\tau$, nondimensional pressure coefficient $C_p = (p - p_0)/\rho \hat{u}_\tau^2$ and nondimensional pressure gradient $\beta = (\nu/\rho \hat{u}_\tau^3)(\partial p/\partial x)$ along the bottom wall in one pitch

Results and discussion

The following discussion focuses on the flow in the lower half of the flow passage; i.e., in the half region of the solid wall side.

Mean flow

The streamwise variation of the friction velocity $\hat{u}_\tau^+ (= u_\tau/\hat{u}_\tau)$, the nondimensional pressure coefficient $C_p = (p - p_0)/\hat{\rho}\hat{u}_\tau^2$, and the pressure gradient $\beta = (\nu/\rho \hat{u}_\tau^3)(\partial p/\partial x)$ over one pitch along the bottom wall are given in Figure 2. Each is found to vary periodically along the bottom wall. Because there is a constant negative value of β in a sink flow, it is suggested that relaminarization occurs at β below -0.025 (Spalart 1986). However, in the present flow, a strong favorable pressure gradient ($\beta < -0.025$) is found in the region $0.06 \leqslant x/H_x \leqslant 0.4$, and no relaminarization is found anywhere (flow data are shown later in the paper).

One of the most interesting features of the pressure gradient effect is the distribution of the mean velocity $\bar{u}/u_\tau$ in sections normal to the wall, as shown in Figure 3 where the distance y from the wall is nondimensionalized as $y^+ = yu_\tau/\nu$ using the local friction velocity u_τ. In the figure, the straight line is the usual log-law given by

$$\bar{u}/u_\tau = 2.5 \log_e y^+ + 5.5 \qquad (2)$$

Experimental findings (Miyake and Nakashima 1993) show that $\bar{u}/u_\tau$ is everywhere above the usual log-law line for flat channel flow and approaches it more closely in the favorable pressure gradient region than in the adverse pressure gradient region. From Figure 3, it is seen that the trend of the curves due to pressure gradient is consistent with the experiment, but the numerical prediction differs from the experimental results in that the curves come below the usual log-law line in the favorable pressure gradient region ($x/H_x = 1/8, 2/8, 3/8$).

Although both the experiments and the present DNS indicate that the mean velocity approaches to the usual straight line in the favorable pressure gradient region and departs from it in the adverse pressure region, in the sink flow boundary layer of constant favorable pressure gradient, the opposite effect was reported by Spalart (1986). This implies that the varying pressure gradient affects a channel flow in a manner fundamentally different from a uniform pressure gradient.

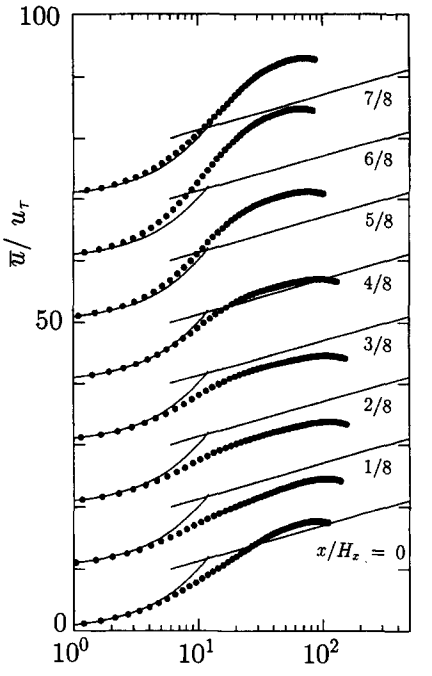

Figure 3 Distribution of mean velocity $\bar{u}$ in vertical sections; u_τ is local friction velocity on the bottom wall

Figure 4 shows the isocontour lines of various quantities averaged in the spanwise direction, in a vertical section of one period. The upper horizontal line is the line of $y = \delta$, and the vertical scale has been doubled. Streamwise variations of various quantities manifest themselves with a phase lag that is closely coincident with the results of previous the LES study (Kajishima and Miyake 1992), suggesting that the truncation of small scale eddies in LES does not significantly affect the global distribution of turbulence quantities. Hence, the discussions given in that work are valid also for this DNS, as a whole. Some additional discussion concerning isocontour lines is given in the following section.

In the acceleration stage, the earliest response appears in the increased production rate of turbulent energy $\hat{P}_k^+ = P_k/(\hat{u}_\tau^4/\nu)$ in the layer close to the wall, and then the turbulent energy k itself follows. $\hat{P}_k^+$ begins to be enhanced near the section where $d\beta/dx$ crosses zero from negative to positive ($x/H_x \simeq 0.23$) and attains its maximum value at the midsection of decelerating region. Turbulent energy itself varies in parallel with the production rate, but with a phase delay in the streamwise direction and reaches its peak value at the section downstream of that of the maximum production rate.

Table 1 Computational conditions

	Streamwise, x	Wall-normal, y	Spanwise, z
Length, H	$4\pi\delta$	2δ	$\pi\delta$
Grid number, N	128	129	64
Grid separation (h/δ)	$h_x = 0.098$	$h_y = 0.00030 \sim 0.024$	$h_z = 0.049$
Grid separation (h^+)	$h_x^+ = 14.7$	$h_y^+ = 0.045 \sim 3.68$	$h_z^+ = 7.36$
Mode	Fourier	Chebyshev	Fourier
Reynolds number		$Re_\tau = \delta \bar{u}_\tau/\nu = 150$	

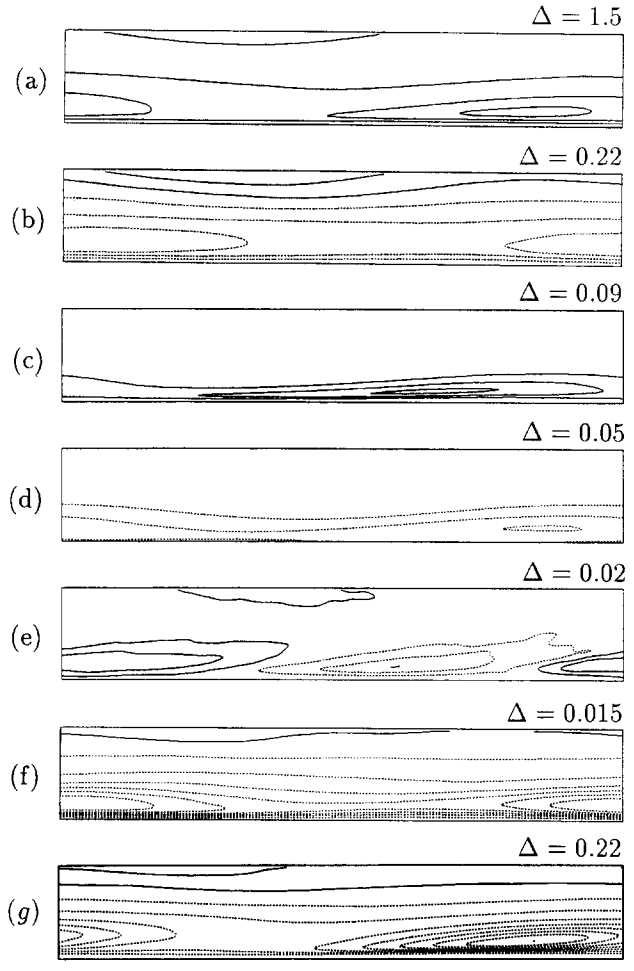

Figure 4 Isocontours of various statistical quantities of turbulence in a vertical section of lower half region of flow passage: (a) = turbulent kinetic energy $\hat{k}^+$; (b) = turbulent shear stress $\overline{u'v'}/\hat{u}_\tau^2$; (c) = production rate of turbulent kinetic energy $\hat{P}_k^+$; (d) = dissipation rate of turbulent kinetic energy $\hat{D}_k^+$; (e) = convection rate of turbulent kinetic energy $\hat{C}_k^+$; (f) = production rate $\hat{P}_{12}^+$ of turbulent shear stress; (g) = turbulent shear stress $\overline{u'v'}$ based on à priori test by Nagano and Shimada model (1993). Increments of neighboring lines are given at the top right corners; length scale is the same as in Figure 2

In the section farther downstream, the shear stress $-\overline{u'v'}/\hat{u}_\tau^2$ reaches its peak value. This delay in the enhancement of the shear stress downstream relative to that of the turbulent energy has also been confirmed by experiment (Miyake and Nakashima 1993). This delay is interpreted as the distance needed for quasistreamwise eddies to mature, because a large part of the shear stress is generated by the break-up of eddies due to a burst that takes place at the tail of the quasistreamwise eddies after they have matured.

The delay in the turbulent energy relative to its production rate mentioned above can be explained as follows. The production rate of turbulent energy is

$$\hat{P}_k^+ = -\frac{2}{\hat{u}_\tau^4/\nu}\left[\left(\overline{u'^2}-\overline{v'^2}\right)\frac{\partial \bar{u}}{\partial x}+\overline{u'v'}\left(\frac{\partial \bar{u}}{\partial y}+\frac{\partial \bar{v}}{\partial x}\right)\right] \qquad (3)$$

The second term in [ ] is negative everywhere in this flow, and the first term contributes mainly to the streamwise variation of $\hat{P}_k^+$. Because in the first term representing the contribution of normal stress, $\partial\bar{u}/\partial x$ is positive in the acceleration region, it weakens the production rate there, and vice versa. Because $\partial\bar{u}/\partial x$ takes its largest value near the middle of the accelerating region, the enhancement of the production rate starts there and gradually increases in the downstream direction. The production rate attains its peak value in the middle of the decelerating region, where $\partial\bar{u}/\partial x$ attains its most negative value.

The turbulent energy $\hat{k}$ at a given section reflects the streamwise integration of the production rate $\hat{P}_k^+$, although losses such as that lost to convection $\hat{C}_k^+$, which is intensified in the high $\hat{P}_k^+$ region, as shown in Figure 4e, must be taken into account. Consequently, the intensity variation of $\hat{k}$ is delayed relative to that of $\hat{P}_k^+$, thus showing the phase lag. On the other hand, the shear stress shows no phase lag relative to the production rate, as observed in Figure 4b and 4f.

The shift in the peak points of the ingredients of the turbulent energy transport equation shown in Figure 4 depends on the Reynolds number, the wave length of the pressure variation, etc., as the authors' experiment (Miyake and Nakashima 1993) demonstrated. In the experiment, which was at $Re_\tau = 750$, it was found that, although the start of enhancement of $\hat{k}$ was at a section in the accelerating region, the location of the peak points for $\hat{k}$ and $\overline{u'v'}/\hat{u}_\tau^2$ was more upstream than in the present DNS. This is partly because in the higher Reynolds number flow, the size of each event in comparison with the passage dimension becomes smaller than in lower Reynolds number case and that the wave length in wall unit of the DNS is $\lambda\hat{u}_\tau/\nu = 1540$, while in the experiment, it is 9170. However, the qualitative conclusion that the local pressure gradient cannot be used as unique parameter to predict the flow pattern of this type of flow; i.e., consecutively varying internal flow, is to be noted. Production rate is suppressed in the accelerating region and is enhanced in the decelerating region, in parallel with the magnitude of local pressure gradient.

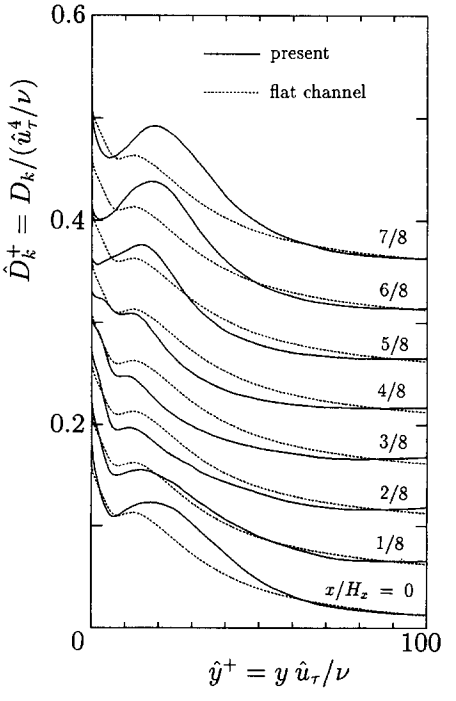

Figure 5 Distributions of dissipation rate of turbulent kinetic energy $\hat{D}^+$ in cross sections; solid lines = DNS; dotted lines = flat channel (Kasagi et al. 1992)

The peak of $\hat{P}_k^+$ approaches closer to the wall in the acceleration region and approaches most closely at the section $x/H_x \simeq 2/8$, where β is at its minimum. Inversely, it moves away from the wall in the deceleration region. This indicates that the flow is pushed toward the wall by the strong positive pressure gradient in the accelerating region and is forced away from the wall in deceleration region.

Figure 5 shows the turbulence energy dissipation rate $\hat{D}_k^+ = D_k/(\hat{u}_\tau^4/\nu)$. In this figure, the broken line indicates the flat channel case of $\mathrm{Re}_\tau = 150$ (Kasagi et al. 1992). The global distribution shown in Figure 4(d) suggests that it varies synchronously with the turbulent kinetic energy. That is, the dissipation increases as the kinetic energy does and vice versa. However, closer examination reveals some peculiar aspects.

Except for the layer very close to the wall, the dissipation rate is attenuated in the accelerating region and is enhanced in the decelerating region, similar to $\hat{P}_k^+$ behavior. The delay in the dissipation response relative to the pressure gradient, however, is more than that of $\hat{P}_k^+$, because the large part of the turbulent energy produced in the strong decelerating region is not dissipated immediately, but rather is brought downstream by the mean flow convection. As a result, the turbulent energy to be dissipated in the downstream section increases. This corresponds to the fact that whereas production is governed by large scale eddies, dissipation is governed by small ones, and the break-down of eddies to successively smaller ones by the cascade mechanism needs time.

In the layer very close to the wall, the response is rapid. That is, it varies almost synchronously with the pressure gradient. In addition, the complex profile of the curves appears from $x/H_x = 3/8$ to $5/8$. The very rigorous requirement of the asymptotic behavior of the dissipation rate model may be excessive for this flow.

Furthermore, in Figures 4c and 4d, it is found that the streamwise variation of the dissipation rate is smaller than that of the production rate. Therefore, it is concluded that the periodic pressure gradient has less influence on the small-scale eddies than on the large-scale ones, which may explain why LES gives reasonable results for this flow, even if the small scale eddies are replaced by a primitive model.

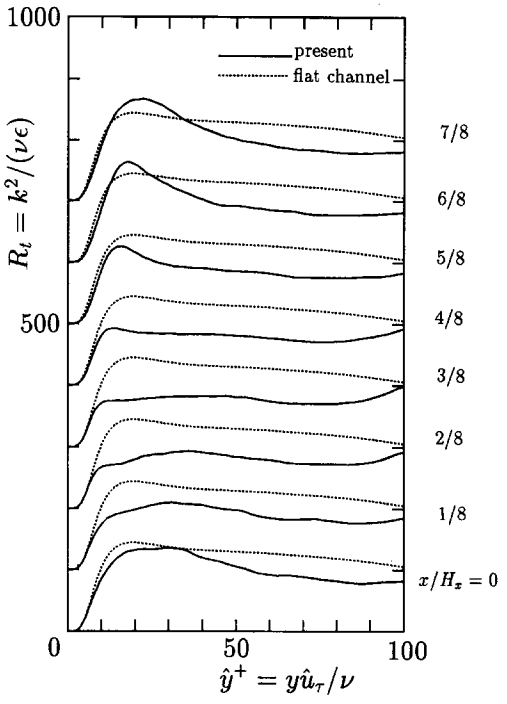

Figure 6 Distributions of turbulent Reynolds number $R_t = k^2/(\nu\epsilon)$ in cross sections; solid lines = DNS; dotted lines = flat channel (Kasagi et al. 1992)

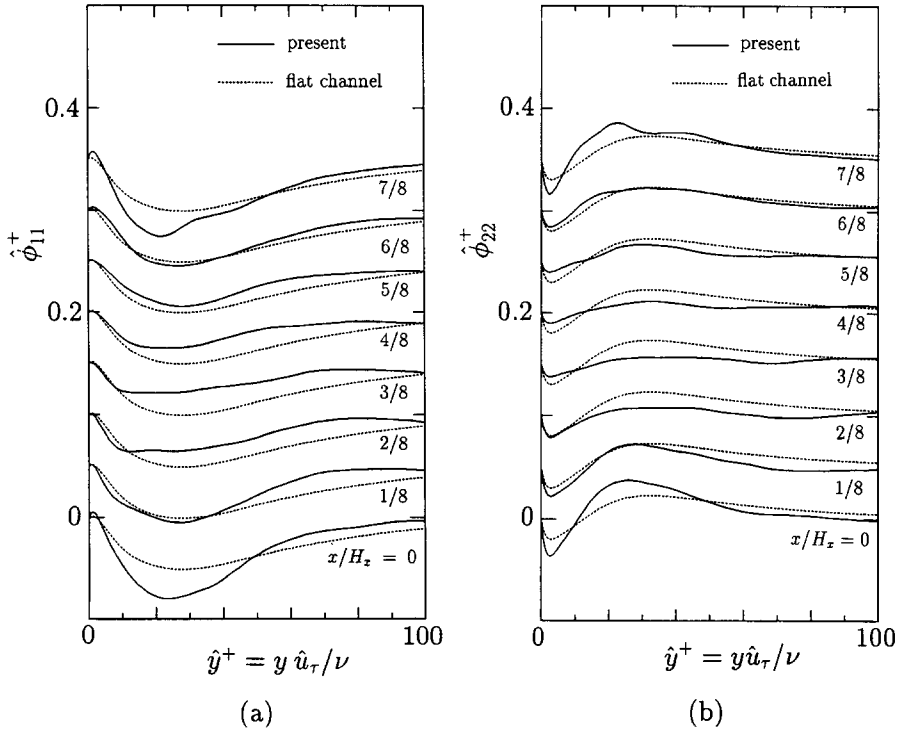

Figure 7 Distributions of redistribution terms in cross sections: (a) = ϕ_{11}^+; (b) = ϕ_{22}^+; solid lines = DNS; dotted lines = flat channel (Kasagi et al. 1992)

The most striking difference between this DNS and the flat channel case is found in the cross-sectional distribution of turbulent Reynolds number $R_t = k^2/\nu\epsilon$, which is shown in Figure 6. Because in eddy-viscosity-type models, the turbulent eddy-viscosity is usually defined as $\nu_t/\nu = C_\mu f_\mu R_t$ where C_μ, f_μ are model constant and the wall damping function, respectively, the curves shown in the figure are proportional to ν_t. Obviously, in this flow ν_t, accordingly the strength of turbulent mixing, is much weaker than in the flat channel case in the core region of the flow passage. The difference in the proportion of wall friction on the two walls makes the turbulence property different in the region above the buffer layer from the flat channel case, even if the friction velocities are identical. Namely, when the quantities are reduced to wall variables, the similarity between the two flows are limited within a very thin layer.

The lowering of ν_t is mainly due to the decline of k in the core region, which is caused by the relative rise in the total dissipation rate in one pitch. Namely, the excess turbulent energy production in the diverging region is convected downstream by the mean flow and is dissipated in the converging region where the dissipation rate becomes greater than it should be for the production rate there. Therefore, the high production of turbulent energy in the diverging region is less effective in enhancing the turbulent energy and does not compensate for its reduction in the converging region.

Figure 7 shows examples of cross-sectional profiles of the redistribution terms (a) ϕ_{11}^+ and (b) ϕ_{22}^+. The dotted lines again indicate the flat channel flow. It should be noted that both ϕ_{11}^+ and ϕ_{22}^+ in the region above the buffer layer are remarkably enhanced in phase with the shear stress $|\overline{u'v'}|$ and the production rate of shear stress P_{12}. Namely, redistribution terms are enhanced where these terms become stronger than in a flat channel flow and are strongly attenuated in the region from midacceleration to mid-deceleration sections, indicating that the underlying physical phenomenon of redistribution terms are related to the generation of turbulent shear stress. The mechanism of the redistribution phenomenon is interpreted as the flow deflection induced by the high-pressure spots generated by the quasistreamwise eddies around their cores (Iida and Kasagi 1993). The above-mentioned distributions of the redistribution terms support this interpretation and suggest that enhancement of the quasistreamwise eddies is crucially important to the near-wall turbulence, which, in turn, is strongly influenced by the mean pressure gradient.

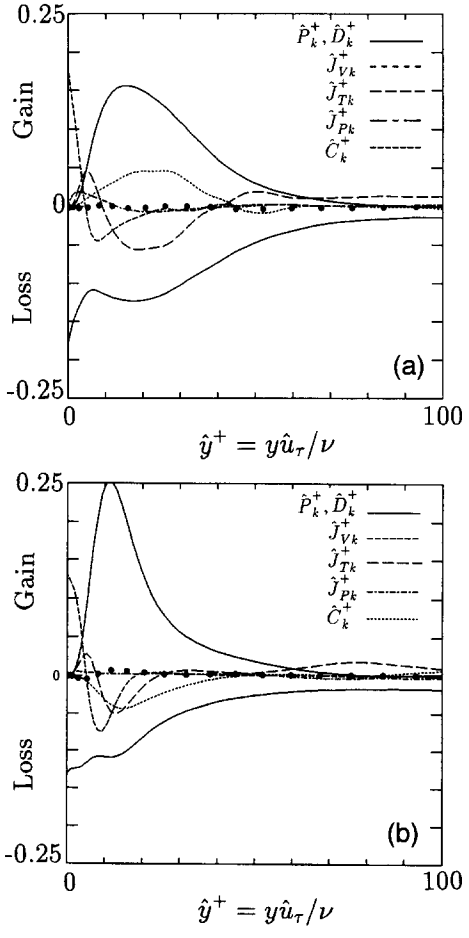

Figure 8 Budget of transport equation of turbulent kinetic energy; (a) = $x/H_x = 0$; (b) = $x/H_x = 2/4$; ● indicates the residual

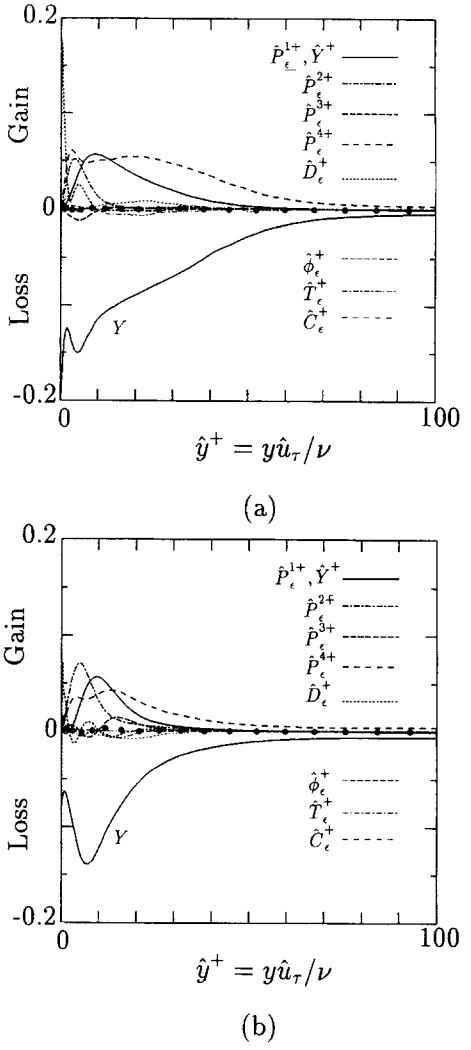

Figure 9 Budget of transport equation of dissipation rate of turbulent kinetic energy; (a) = $x/H_x = 0$; (b) = $x/H_x = 2/4$; ● indicates the residual

Budget of Reynolds stress transport equation

In this section, we present examples of the budget of the transport equations for Reynolds stress. The budget of the turbulent kinetic energy k and its dissipation rate ϵ are shown, because they are typical and important quantities in turbulence models.

The budget of the turbulent kinetic energy is given in Figure 8 in which all the quantities are nondimensionalized as wall variables using $\hat{u}_\tau$ and ν. Figure 8a is for the section of the smallest mean velocity $x/H_x = 0$ and Figure 8b, for that of the largest mean velocity $x/H_x = 2/4$.

Although numerical accuracy in the previous LES (Kajishima and Miyake 1992) was not high enough to allow testing of turbulence models, and dissipation rate in particular, the present DNS is sufficiently accurate, as shown by the residuals of the budget given by ● in the figures, which are negligibly small at every point in each of the sections.

In the budget of turbulent kinetic energy, the production rate, and the dissipation rate are almost in balance locally, as in the flat channel flow, but in this particular flow, convection absorbs a large part of the excess or deficit of production over dissipation. Furthermore, the diffusion term plays a more important role and extends farther away from the wall than in the flat channel case. The streamwise variation of turbulence is mostly an enhancement of diffusion. The turbulent energy transported farther away from the wall by diffusion is convected downstream by the mean flow.

Figure 9 shows the budget of the transport equations of energy dissipation rate ϵ in which terms are identical with those defined in Mansour et al. (1988); i.e., $\hat{P}_\epsilon^+$ are production terms of dissipation $\hat{D}_\epsilon^+$, viscous diffusion $\hat{\phi}_\epsilon^+$, pressure transport $\hat{T}_\epsilon^+$, turbulent transport $\hat{Y}^+$, dissipation, and $\hat{C}_\epsilon^+$ convection. The nondimensionalization is the same as in Figure 8 and also the meaning of the symbol ● is the same. It is found that the numerical accuracy is sufficient to satisfy the required balance.

Dissipation $\hat{Y}^+$ is the major term in the ϵ-transport equation, and it is modified seriously by the nonuniform mean flow, but the terms $\hat{\phi}_\epsilon^+$, $\hat{T}_\epsilon^+$, $\hat{D}_\epsilon^+$ are quite small at every section and are insensitive to the mean flow fluctuation. The production term fluctuation from one section to the other is large.

A typical property of the eddy-viscosity-type turbulence models is demonstrated in Figure 4(g), which shows the isocontour map of turbulent shear stress obtained by an eddy-viscosity model of Nagano and Shimada (1993), which gives the eddy-viscosity as $\nu_t = C_\mu f_\mu k^2/\epsilon$ where $C_\mu = 0.09$, $f_\mu = [1 - \exp\{-(y^+/44)^2\}][1 + 45/R_t^{3/4}\exp\{-(R_t/55)^{1/2}\}]$, $R_t = k^2/\nu\epsilon$. In the calculation of Figure 4g, the rate of strain, k and ϵ are brought from this DNS. As mentioned before, no phase shift appears between the production rate of the turbulent shear stress and shear stress itself, unlike the turbulent kinetic energy or the normal stresses.

Comparing Figure 4g with Figure 4a, we find that the model gives the distribution of $\overline{u'v'}$, which is almost in phase with the turbulent kinetic energy. However, Figure 4b of the present DNS shows that $-\overline{u'v'}$ is enhanced with a phase delay in the downstream direction relative to k. This discrepancy is caused by the fact that eddy-viscosity-type turbulence models calculate both normal and shear stresses using a single relationship between the eddy-viscosity and the rate of strain. It demonstrates that the memory effect, which is, in principle, incorporated in the transport equation of k and ϵ, is not adequately taken into account, as is inferred from the mechanism of the phase delay in the production of the shear stress. In this regard, the eddy-viscosity-type models may have an inherent drawback for flows having pressure variation in the streamwise direction.

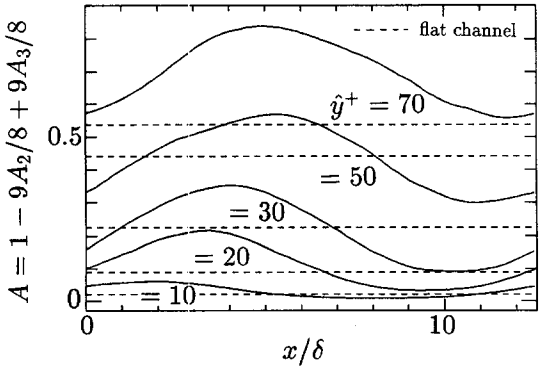

Figure 10 Streamwise variation of flatness parameter A on constant $\hat{y}^+$ surfaces. $A = 1 - 9A_2/8 + 9A_3/8$, $A_2 = b_{ij}b_{ij}$, $A_3 = b_{ij}b_{jk}b_{ki}$, $b_{ij} = \overline{(v_i u_j)}/k - (2/3)\delta_{ij}$

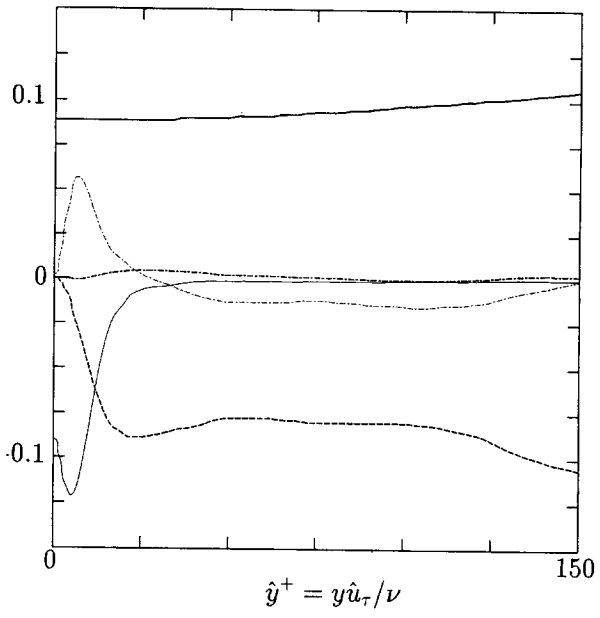

(a)

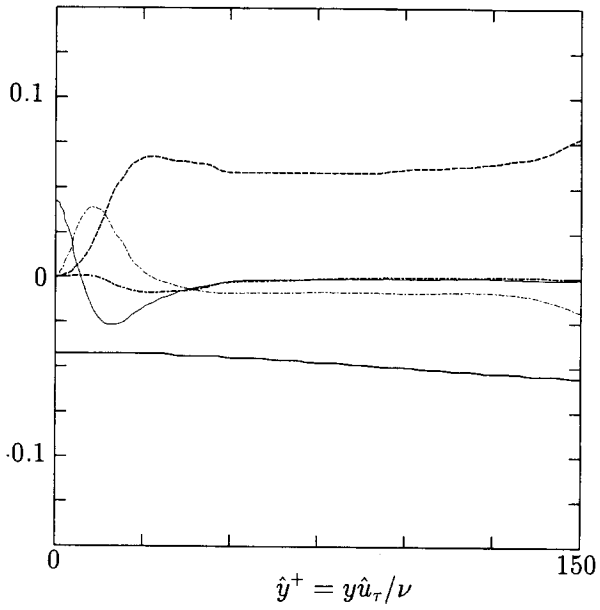

(b)

Figure 11 Momentum balance in streamwise direction; (a) = $x/H_x = 1/4$; (b) = $x/H_x = 3/4$; ———; $-d\overline{p}/dx/(\hat{u}_\tau^3/\nu)$, ———; $-\nu(\partial^2\overline{u}/\partial x^2 + \partial^2\overline{u}/\partial y^2)/(\hat{u}_\tau^3/\nu)$, -----; $-(\partial\overline{uu}/\partial x + \partial\overline{uv}/\partial y)/(\hat{u}_\tau^3/\nu)$, — - — -; $-\partial\overline{u'u'}/\partial x/(\hat{u}_\tau^3/\nu)$, — - — -; $-\partial\overline{u'v'}/\partial y/(\hat{u}_\tau^3/\nu)$

In many turbulence models, the flatness parameter (Lumley 1978) $A = 1 - 9A_2/8 + 9A_3/8$, where A_2 and A_3 are $A_2 = b_{ij}b_{ij}$, and $A_3 = b_{ij}b_{jk}b_{ki}$, $b_{ij} = (\overline{u_i'v_j'})/k - (2/3)\delta_{ij}$, is often used to incorporate the characteristics of turbulence. Figure 10 shows its distribution along a constant y^+ line. Again, the horizontal broken lines are used to indicate the flat channel flow. A is a measure of the three-dimensionality of turbulence and vanishes as the turbulence becomes 2-D. In the decelerating region, where the activity of streamwise eddies becomes enhanced, it is expected intuitively that the three-dimensionality will also be enhanced, but Figure 10 suggests that the opposite is true.

Budget of momentum equation

This section presents a budget of the momentum equation. Figure 11 shows examples of the budgets for the streamwise momentum at the sections $x/H_x = 1/4$ and $3/4$. In the region above buffer layer, or at $\hat{y}^+ \geqslant 30$, the pressure gradient and convection terms are nearly in balance, and the other two terms, representing the contributions of the viscous force and the turbulent shear stress, are small. The pressure profile reflects the curvature of the mean streamlines and becomes more uniform close to the wall. The pressure gradient in the layer close to the wall should be exact if we want to have an accurate prediction by simulation. Therefore, the turbulent shear stress plays an important role in determining the whole flow field, although it is small in magnitude as compared with the other two terms in the core region, because the difference between the two leading terms is mainly covered by turbulent shear stress. In addition, the error in one location affects the accuracy of the whole flow field, because the internal flow now under consideration is inherently elliptic. In the boundary-layer flow, this problem does not appear, because the pressure gradient is given and is not an unknown to be determined simultaneously. Therefore, turbulence models must be more accurate in the internal flow than in the boundary-layer flow or in flows that are homogeneous in the main flow direction. In this sense, this flow is a good case to use in investigating the performance of turbulence models.

As is shown in Figure 11, the contribution of the turbulent normal stress $\partial\overline{u'^2}/\partial x$ to the momentum balance is quite small, meaning that for this flow, the thin-layer approximation in which the model for the turbulent stresses is required only for the shear stress and not for the normal stresses is valid. Usually, flows allowing the thin-layer approximation conceal the inherent drawback of low-order models not being able to predict correctly the anisotropy of turbulent normal stresses.

Conclusion

In this paper, a DNS of a channel flow having a periodic pressure gradient in the flow direction is presented. The conclusions are as follows:

(1) In this channel flow having a streamwise periodic pressure variation, statistical quantities of turbulence such as turbulent kinetic energy, shear stress, ingredient terms in the transport equations of kinetic energy, and dissipation rate vary with a spatial phase lag relative to one another, representing their mutual dependence.

(2) The periodic pressure gradient affects the turbulence structure, but the magnitude of its local gradient cannot be considered a unique governing factor to express the modification of the structure. The variation on the wall diffuses outward away from the wall and is convected downstream at the same time, thus constructing a complex laminating structure of turbulence in cross section.

(3) In this flow, the turbulent eddy Reynolds number $R_t = k^2/\nu\epsilon$ is much smaller than in a flat channel flow. This reduces the wall shear stress on the lower flat plate to a value smaller than that in a flat channel flow. This elliptic property that the pressure is not specified but must be determined as a part of the simulation differentiates this flow from boundary-layer flows having pressure gradient.

(4) An inherent drawback of the alignment of tensors of turbulent stress and strain rate is suggested.

(5) The momentum balance shows that although the thin layer approximation is valid for this flow, an error in the prediction of the shear stress in the core region may aggravate the accuracy of prediction of the whole flow.

References

Frederick, K. A. and Hanratty, T. J. 1988. Velocity measurements for a turbulent nonseparated flow over solid waves. *Exp. Fluids*, **6**, 477–486

Hunt, J. C. R., Newley, T. M. J. and Weng, W. S. 1990. Analysis and computation of turbulent boundary layers with varying pressure gradients. In *Computational Methods in Aeronautical Fluid Dynamics*, P. Stow (ed.), Clarendon, pp. 59–91

Iida, O. and Kasagi, N. 1993. Redistribution of the Reynolds stresses and destruction of the turbulent heat flux in homogeneous decaying turbulence. *Proc. 9th Symposium on Turb. Shear Flows*, Kyoto, Japan, Aug. 16–18, 24-4-1–24-4-6

Kajishima, T. and Miyake, Y. 1992. Large-eddy simulation of a turbulent channel flow with a periodic pressure gradient. *JSME Intern. J., Ser. II*, **35**, 23–28

Kasagi, N. et al. 1992. Establishment of the direct numerical simulation data bases of turbulent transport phenomena. Cooperative Research No. 02302043 supported by the Ministry of Education, Science and Culture

Kim, J., Moin, P. and Moser, R. D. 1987. Turbulence statistics in fully developed channel flow at low Reynolds number. *J. Fluid Mech.*, **177**, 133–166

Lumley, J. L. 1978. Computational modeling of turbulent flows. *Advances Appl. Mech.*, **18**, 123–176

Mansour, N. N., Kim, J. and Moin, P. 1988. Reynolds-stress and dissipation-rate budgets in a turbulent channel flow. *J. Fluid Mech.*, **194**, 15–44

Miyake, Y. and Nakashima, M. 1993. An experiment of a turbulent flow in a wavy channel. In *Exp. Heat Transf. Fluid Mech. Thermdyn.*, Kelleher et al. (eds.), 1034–1041

Nagano, Y., Tagawa, M. and Tsuji, T. 1993. Effects of adverse pressure gradients on mean flows and turbulence statistics in a boundary layer. In *Turbulent Shear Flows*, F. Durst et al. (eds.), Springer-Verlag, Berlin, 7–21

Nagano, Y. and Shimada, M. 1993. Modeling the dissipation-rate equation for wall shear flows (Comparison with direct simulation data). *Trans. JSME*, Ser. B, **59**, 559, 742–749

Patel, V. C., Chon, J. T. and Yoon, J. Y. 1991. Turbulent flow in a channel with a wavy wall. *J. Fluid Eng., Trans. ASME*, **113**, 579–586

Sano, M. 1992. Fluid flow and heat transfer in a periodically diverging–converging turbulent channel flow. *Trans. JSME*, Ser. B, **58**, 1386–1391

Sano, M. and Asako, Y. 1991. Fluid flow and heat transfer in a periodically diverging–converging turbulent duct flow. *Trans. JSME*, Ser. B, **57**, 541, 2962–2969

Spalart, P. R. 1986. Numerical study of sink-flow boundary layers. *J. Fluid Mech.*, **176**, 307–328

Zeman, O. and Jensen, N. O. 1987. Modification of turbulence characteristics in flow over hills. *Quart. J. Roy. Meteorol. Soc.*, **113**, 55–80